Know Thy Nano Neighbor. Plasmonic *versus* Electron Charging Effects of Metal Nanoparticles in Dye-Sensitized Solar Cells

Hyunbong Choi,[†] Wei Ta Chen,[†,‡] and Prashant V. Kamat[†,*]

[†]Radiation Laboratory, Departments of Chemistry and Biochemistry and Chemical & Biomolecular Engineering, University of Notre Dame, Notre Dame, Indiana 46556, United States and [‡]Department of Materials Science and Engineering, National Chiao Tung University, Hsinchu, Taiwan 30010, Republic of China

ABSTRACT Neighboring metal nanoparticles influence photovoltaic and photocatalytic behavior of semiconductor nanostructures either through Fermi level equilibration by accepting electrons or inducing localized surface plasmon effects. By employing SiO_2- and TiO_2-capped Au nanoparticles we have identified the mechanism with which the performance of dye-sensitized solar cells (DSSC) is influenced by the neighboring metal nanoparticles. The efficiency of an N719 dye-sensitized solar cell (9.3%) increased to 10.2% upon incorporation of 0.7% Au@SiO_2 and to 9.8% upon loading of 0.7% Au@TiO_2 nanoparticles. The plasmonic effect as monitored by introducing Au@SiO_2 in DSSC produces higher photocurrent. However, Au nanoparticles undergo charge equilibration with TiO_2 nanoparticles and shift the apparent Fermi level of the composite to more negative potentials. As a result, Au@TiO_2 nanoparticle-embedded DSSC exhibit higher photovoltage. A better understanding of these two effects is crucial in exploiting the beneficial aspects of metal nanoparticles in photovoltaics.

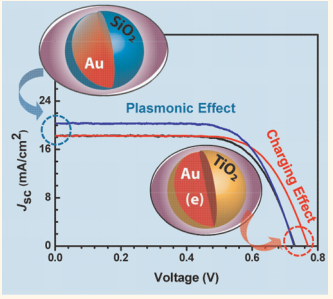

KEYWORDS: semiconductor–metal composite · photocatalysts · TiO_2 · core–shell nanoparticles · localized surface plasmon · solar energy conversion · electron storage · Fermi level equilibration

Semiconductor nanoparticles have been extensively used in the design of next-generation solar cells[1−3] and photocatalysts for water splitting[4−7] and environmental remediation.[8] In recent years surface plasmon resonance of metal nanoparticles has been regarded as an attractive approach to boost the performance of semiconductor nanostructure-based light-harvesting assemblies.[9−14] For example, by coupling semiconductor nanostructures with nanoparticles in a core–shell geometry one can observe an enhancement in their photocatalytic or photovoltaic behavior. A variety of explanations have been presented in these studies to explain the observed improvement in photoconversion efficiency. These include (i) increased absorption due to surface plasmons and light-trapping effects, (ii) improved charge separation as a result of localized electromagnetic field, (iii) promoting electron transfer to adsorbed species, and (iv) electron storage effects that can drive the Fermi level to more negative potentials.

The marriage between semiconductor and metal nanoparticles in photocatalysis dates back to the 1970s, when efforts were made to generate hydrogen using photo-assisted catalysis.[15−23] Since then, many studies have focused on the role of metal nanoparticles as a cocatalyst in facilitating electron discharge and reduction of H^+ or other species at the interface.[7,24−29] While metals such as Pt quickly discharge electrons to the surrounding medium, metal nanoparticles such as Ag and Au store a fraction of electrons captured from photoexcited semiconductor nanoparticles.[30−34] Double-layer charging has been shown to play a role in stabilizing stored electrons within the metal nanoparticles.[35−37] The storage of electrons, which depends on the size of the metal nanoparticles, undergoes charge equilibration with a photoexcited semiconductor and drives the Fermi level to more negative potentials. For example a shift of 60–100 mV in the Fermi level (and hence the photovoltage) is seen when TiO_2 films were coupled with size-selective gold nanoparticles.[34] Another influence of such electron storage is the suppression of back electron transfer. For example, in a photosensitization experiment, such Ag@TiO_2 particles have been shown to reduce charge recombination

* Address correspondence to pkamat@nd.edu.

Received for review March 14, 2012 and accepted April 11, 2012.

Published online April 11, 2012
10.1021/nn301137r

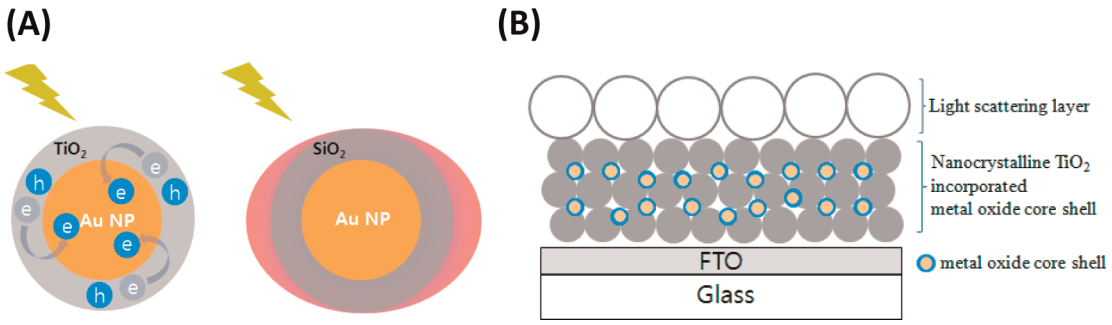

Scheme 1. (A) Charging effect (Au@TiO_2) *versus* plasmonic effect (Au@SiO_2) of metal core−oxide shell particles. (B) Schematic drawing depicting the layered structure of a mesoscopic TiO_2 film incorporating core−shell particles typically employed for high-efficiency DSSC.

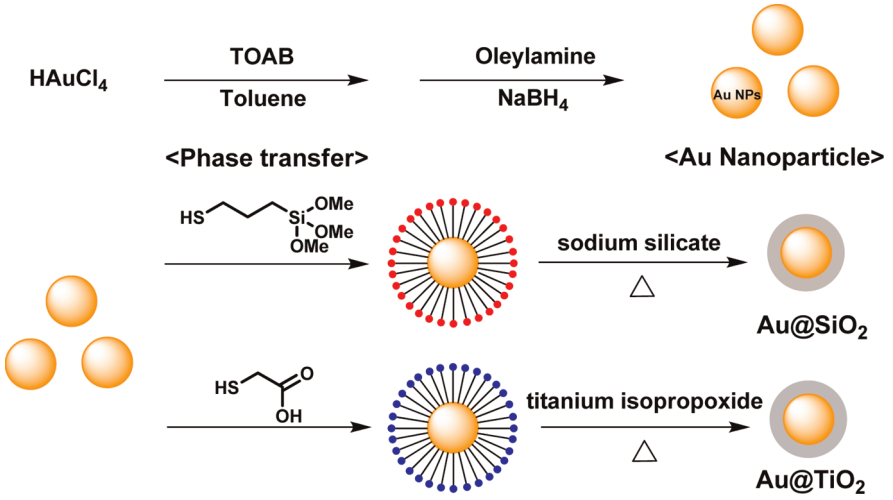

Scheme 2. Synthesis of Au core oxide shell structures.

between the injected electron and oxidized sensitizer.[38]

A convenient way to probe the electron storage in metal nanoparticles is by monitoring its plasmon frequency. The accumulation of electrons within silver and gold nanoparticles or nanorods causes a blue-shift in the absorption spectrum due to the increasing surface plasmon frequency of the electron gas.[39,40] Thus, the correlation between the number of stored electrons and the shift in plasmon frequency provides a good measure to establish the mechanism with which electron charge and discharge cycles operate in a semiconductor-assisted photocatalytic system.

Metal nanoparticles such as silver and gold exhibit surface plasmons, creating an intense electromagnetic field in the immediate vicinity.[41−47] Such localized surface plasmon resonance, which has been well captured in surface-enhanced Raman spectroscopy (SERS), can be manipulated to influence charge separation by placing the semiconductor nanoparticles near the plasmonic metal nanoparticles.[46] In addition, the metal nanoparticles enhance the light absorption of semiconductor nanostructures, thus enabling better photon management in photovoltaics.[9,11,48] Many recent studies that employ Ag@TiO_2 or Au@TiO_2 in solar cells and photocatalysis have attributed the improved photoconversion efficiency exclusively to surface plasmon effects.[9,13,49−52] Similarly, enhancement seen in the photocurrent generation of iron oxide-coated gold nanopillars and water splitting reaction with gold nanoparticles deposited on Fe_2O_3 photoanodes has been attributed to surface plasmon resonances and photonic-mode light trapping.[46,50] No effort was made in these studies to include or exclude photocharging effects that would arise from storage of electrons within the metal core. As shown in a recent review, the plasmonic effect coupled with electron charging of metal particles plays an important role in the operation of semiconductor−metal devices.[53] In addition, if the semiconductor (*e.g.*, CdSe) is quantized, the strong coupling between the lowest excited state or excitonic transition and surface plasmon of the neighboring metal surface needs to be taken into account.[54,55]

The focus of the present study is to isolate the plasmonic and charging effects by capping the Au nanoparticles with SiO_2 and TiO_2, respectively, and track their influence in a dye-sensitized solar cell. SiO_2, being an insulator, acts as a barrier to prevent electron charging of the metal core, thus exhibiting only surface plasmon effects. On the other hand TiO_2,

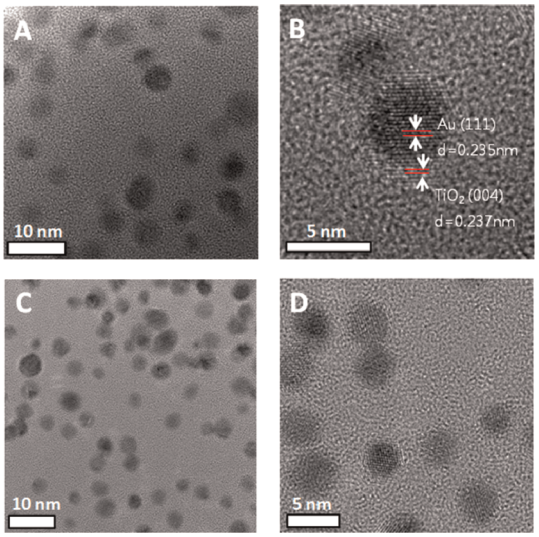

Figure 1. TEM and HRTEM images of (A, B) Au@TiO_2 and (C, D) Au@SiO_2 NPs.

being a semiconductor, is capable of transferring electrons to the Au core and thus charges the core in Au@TiO_2 core@shell nanoparticles. By incorporating Au core@metal oxide shell nanoparticles in the dye-sensitized solar cells (DSSC), we have succeeded in identifying the influence of these effects.

RESULTS AND DISCUSSION

Synthesis and Characterization of Au@TiO_2 and Au@SiO_2. The metal core−oxide shells were synthesized using a stepwise synthetic protocol as summarized in Scheme 2. Metal core−oxide shell structures were prepared by a three-step synthesis that involved reduction of metal ions, exchange of surface ligand, and hydrolysis of titanium isopropoxide and sodium silicate as the TiO_2 and SiO_2 precursor, respectively.

The TEM images of two different core−shell structures are presented in Figure 1. In both cases the Au core was similar, with a particle diameter of 5−6 nm. All particles have a very thin capping of a TiO_2 or a SiO_2 shell of thickness in the range 0.7−1.0 nm. The presence of the TiO_2 shell was confirmed from the grating pattern. Further evidence for the core−shell structure was obtained by performing an energy dispersive X-ray analysis (see Supporting Information).

The particle concentration was estimated by assuming a uniform distribution of Au core particles and an average particle size of 5 nm, as obtained from Figure 1A and B. In this work, the concenturation of Au nanoparticles (conc) was 10 mM. The average number of particles was estimated to be 1.559×10^{15} per mL, following eq 1.

$$\text{total \# of Au NPs} = \frac{\text{total \# of moles}}{\text{\# of moles per NP}} = \frac{\text{conc} \times \text{vol}}{4/3\pi r^3 \times d/M} \quad (1)$$

In the above equation, r is the half-diameter of the gold nanoparticle, d is the density of gold, and M is the atomic weight of the gold.

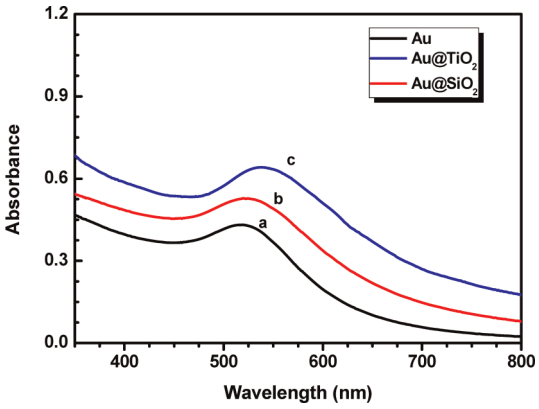

Figure 2. Absorption spectra of (a) Au, (b) Au@SiO_2, and (c) Au@TiO_2 suspension in toluene.

Figure 2 shows the absorption spectra of Au, Au@TiO_2, and Au@SiO_2 colloids in toluene. These three types of particles exhibit surface plasmon absorption in the visible, confirming the plasmonic activity of Au nanoparticles or the Au nanocore. The surface plasmon band of Au@SiO_2 and Au@TiO_2 nanoparticles seen at 527 and 542 nm, respectively, were red-shifted as compared to the Au nanoparticle (518 nm) prepared using the borohydride reduction method. This small shift in the plasmon peak in the case of Au@TiO_2 and Au@SiO_2 colloids is attributed to the oxide shell surrounding the Au nanocore. The higher refractive index of the SiO_2 and TiO_2 shell has been shown to influence the surface plasmon absorption.[56] For a shell thickness of less than 10 nm this red-shift in the absorption is expected to be linear.[9]

Plasmon Response of Au@TiO_2 and Au@SiO_2 Nanoparticles to Steady-State UV-Irradiation. In order to probe the light-induced effects, we subjected the two core@shell nanoparticle suspensions (deaerated) in toluene/ethanol to UV (λ > 300 nm) irradiation. Figure 3A shows the changes in the plasmon absorption following the UV-irradiation of Au@TiO_2 at different times. The plasmon absorption shifts from 530 nm to 516 nm within 15 min of UV-irradiation. The shift of 14 nm in the plasmon absorption band represents increased electron density in the Au core during photoirradiation since the plasmon frequency (ω_p) is directly proportional to the square root of the electron density (N), as illustrated in expression 2,

$$\omega_p = (Ne^2/e_0 m_{eff})^{1/2} \quad (2)$$

where e, ε_0, and m_{eff} are the charge, vacuum permittivity, and effective mass of the free conduction band electrons, respectively.[57]

Under UV-irradiation the electron−hole pairs are generated within the TiO_2 shell. As the holes are scavenged, the electrons are transferred to the Au core (reactions 3 and 4).

$$\text{Au@TiO}_2 + h\nu \rightarrow \text{Au@TiO}_2(e^- + h^+) \quad (3)$$

$$\text{Au@TiO}_2(e^- + h^+) + C_2H_5OH \rightarrow \text{Au}(e)\text{@TiO}_2 + \bullet C_2H_5O \quad (4)$$

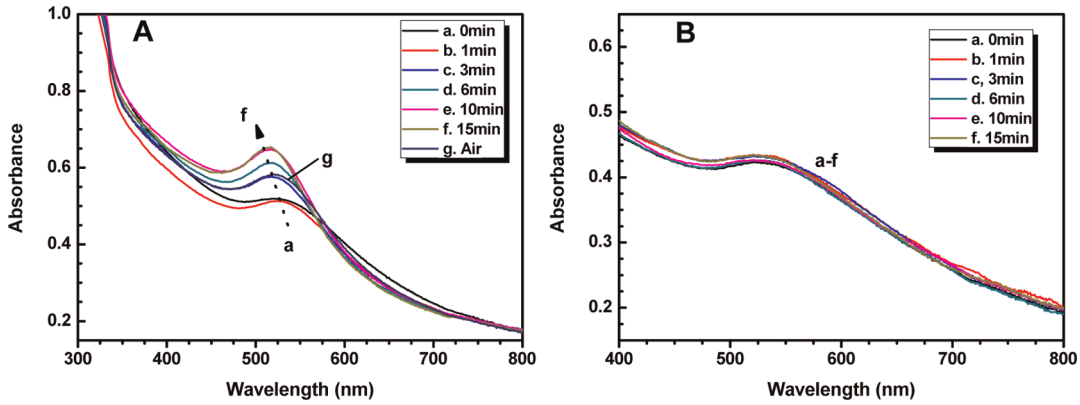

Figure 3. Absorption spectra recorded following UV-irradiation of (A) Au@TiO_2 and (B) Au@SiO_2 colloidal suspensions in toluene/ethanol (1:1): (a) 0, (b) 1, (c) 3, (d) 6, (e) 10, (f) 15 min of UV-irradiation. Spectrum g was recorded after stopping the illumination and exposing it to air.

The $^{\bullet}C_2H_5O$ radical possesses reductive properties and also can donate additional electrons to Au@TiO_2. The Fermi level of Au nanoparticles, though dependent on the particle size, is expected to be close to the value of bulk Au ($E_F = +0.45$ V *vs* NHE). Since this value is more positive than the conduction band of TiO_2 ($E_{CB} = -0.5$ V *vs* NHE), the electrons are readily transferred to the Au core. As the electrons accumulate within the Au core, the Fermi level shifts to more negative potential. This electron transfer between the two continues until the Fermi levels of TiO_2 and Au equilibrate. This observation is consistent with the blue-shift observed with electron storage in gold nanoparticles under reductive conditions. The small gold nanoparticles have the ability to undergo double-layer charging and thus stabilize stored electrons in an inert atmosphere.

To verify the observed plasmon absorption shift was due to the excitation of the semiconductor shell and not by the direct excitation of the metal core, we monitored the absoprtion spectrum of Au@SiO_2 colloids suspended in deaerated toluene/ethanol (1:1) after UV-irradiation. The plasmon absorption band with a maximum at 526 nm remained constant during the UV-irradiation (Figure 3B). SiO_2, being an insulator, does not directly participate in the photoinduced electron transfer process. By comparing these results, we can conclude that the changes in the plasmon absorption band in Au@TiO_2 arise from the shell and not the Au core.

The electrons stored in the Au core could be discharged if we subject the previously irradiated Au@TiO_2 suspension to air. The oxygen quickly scavenges the electrons, restoring the original plasmon absorption. The reproducibility of charging and discharging of electrons in Au@TiO_2 nanoparticles was ascertained by repeating the cycles of UV-irradiation of a deareated suspension followed by exposure to air in the dark. Figure 4 shows the shift in plasmon absorption peak during the irradiation and exposure to air after stopping the illumination. It should be noted that

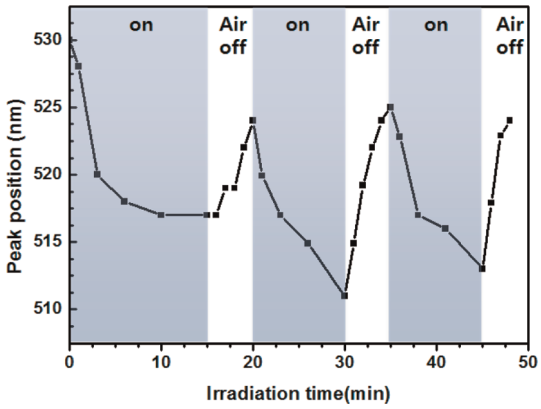

Figure 4. Reversibility of electron storage−discharge cycles: The response of the plasmon absorbance peak was recorded following UV-illumination (charge) of a deaerated Au@TiO_2 colloidal suspension in toluene/ethanol (1:1) and dark discharge in air.

the suspension was deaerated for 20 min before UV-irradiation of each charging cycle to exclude oxygen from the suspension. The reproducibility of a ~15 nm shift during these cycles confirms the ability of Au@TiO_2 nanoparticles to undergo charging when excess electrons are available in the TiO_2 shell.

We also estimated the electron storage capacity of the Au core by titrating with an electron acceptor. We followed the titration procedure adopted earlier of using methylene blue dye as an electron acceptor.[29] Since the reduced dye (two-electron reduction product is stable in inert atmosphere) is colorless, we can add increments of deaerated dye solution in small amounts until dye absorption occurs. From the end point we estimate the ability to store about 600 electrons/per particle of in Au@TiO_2 under equilibrium conditions. Details of the electron titration using thionine dye are given in the Supporting Information. Such large electron storage is in agreement with earlier observations.[30,34,40,58] Such electron storage under Fermi level equilibration conditions renders the Au@TiO_2 nanoparticles more reductive than TiO_2 alone. Now the obvious question that

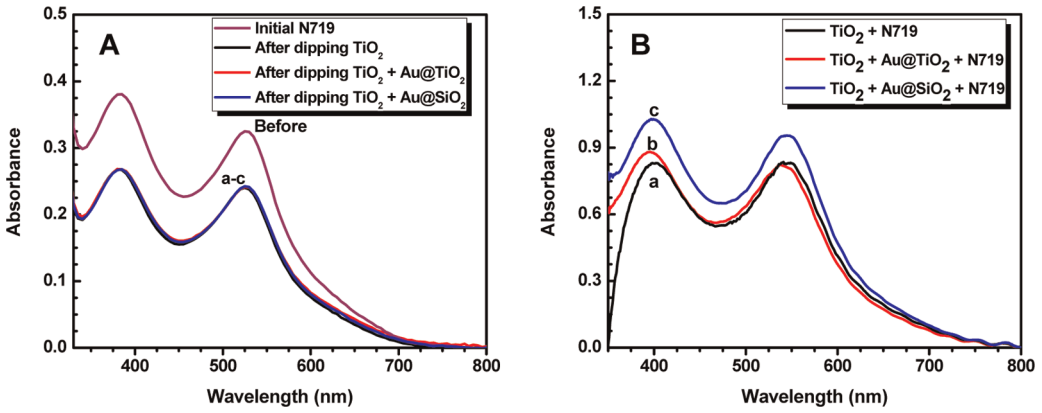

Figure 5. (A) Absorption spectra of N719 in EtOH before and after immersing films of (a) TiO_2, (b)TiO_2/Au@TiO_2, and (c) TiO_2/Au@SiO_2 cast on conducting glass electrodes. (B) Corresponding spectra of the dye adsorbed onto TiO_2 films.

we need to address is how does such electron storage influence the performance of dye-sensitized soalr cells.

Dye-Sensitized TiO_2 Films and the Effect of Gold Nano Neighbor on the Optical Absorption. In a dye-sensitized solar cell dye molecules are anchored on mesoscopic TiO_2 films. In order to assess the effect of Au metal on the performance of DSSC, we incorporated Au@TiO_2 and Au@SiO_2 in two separate TiO_2 pastes. The concentration of these core@shell particles was about 0.7% similar to the composition employed in earlier studies.[11] Each film was prepared by doctor-blading TiO_2 NPs and TiO_2 NPs blended with Au@TiO_2 and Au@SiO_2 NPs on optically transparent electrodes. The electrode prepared with TiO_2 paste alone served as a reference. The annealed electrodes were soaked in dye solution for several hours. The absorption spectra of the dye solution was periodically measured until the desired amount of dye was loaded onto the electrodes. Figure 5A shows the absorption spectra of N719 dye solution before and after immersion of TiO_2 electrodes in three separate sets of experiments. As evident from the difference in the absorption spectra, we were successful in obtaining the same amount of dye loading on each of these three electrodes. The electrodes were then washed with EtOH to remove any physisorbed dye molecules.

The absorption spectra of three dye-loaded TiO_2 films are shown in Figure 5B. The absorption spectra of dye molecules adsorbed onto a pristine TiO_2 film and a TiO_2 film mixed with Au@TiO_2 exhibit similar absorbance features. However the dye adsorbed onto TiO_2 films containing Au@SiO_2 exhibits slightly higher absorption compared to the other two. Despite the same amount of dye loading in these films, the presence of Au@SiO_2 seems to have a noticeable effect on the dye absorption properties. The increase of dye extinction is attributed to the interaction of the dye molecular dipole and the enhanced electromagnetic field induced by localized surface plasmons (LSP). As discussed earlier for a similar system, the increased light absorption of the dye arises from the contributions of resonant energy transfer or near-field coupling between the surface plasmon and the dye-excited state.[11]

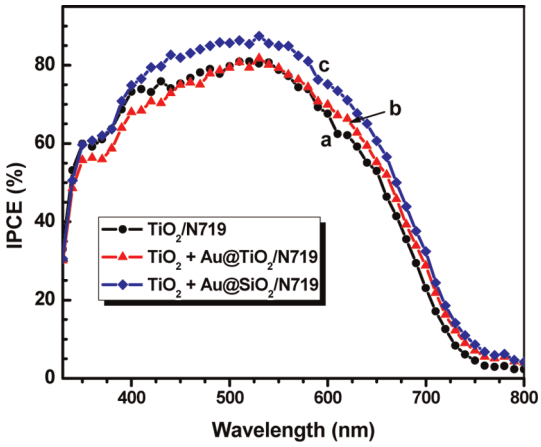

Figure 6. IPCE spectra of DSSC employing N719 adsorbed onto (a) TiO_2, (b) TiO_2/Au@TiO_2, and (c) TiO_2/Au@SiO_2 as photoanodes and platinum counter electrode. The loading of core–shell particles in (b) and (c) was maintained at 0.7%.

Photoelectrochemical Performance of DSSC. If indeed a localized surface plasmon effect is responsible for increased absorptivity, we should be able to observe this effect in the photocurrent action spectra of the electrode in DSSC operation. The N719 dye-loaded TiO_2 films along with the those incorporated with Au@TiO_2 and Au@SiO_2 were employed as photoanodes in a sandwich-type solar cell. The counter electrode was platinum, and the electrolyte consisted of 0.6 M 1,2-dimethyl-3-propylimidazolium iodide, 0.05 M I_2, 0.1 M LiI, and 0.5 M *tert*-butylpyridine in acetonitrile. The photocurrent action spectra recorded in terms of incident photon-to-current conversion efficiency (IPCE) *versus* incident light wavelength are shown in Figure 6. All three electrodes show absorbance in the visible with IPCE (or external quantum efficiency) greater than 80%. Small broadening of the IPCE spectra is seen for TiO_2 films containing Au@SiO_2 and Au@TiO_2 films. However, the films containing Au@SiO_2 show

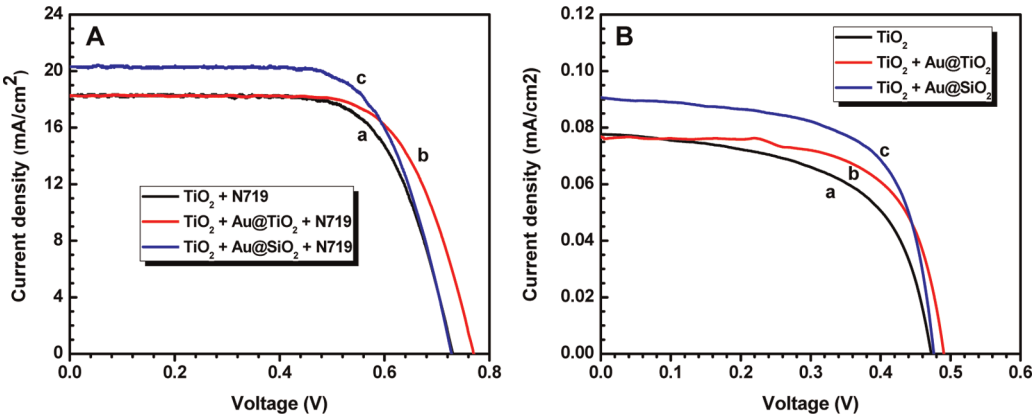

Figure 7. *J*–*V* characteristics of sandwich solar cells. (A) sensitized with dye N719 and (B) without dye configuration: (a) TiO_2, (b) TiO_2/Au@TiO_2, and (c) TiO_2/Au@SiO_2 employed as photoanodes and platinum counter electrode. The TiO_2 films were modified with the dye N719 in (A) and used as is in (B). The solar cell was subjected to AM 1.5 illuminations with a masked area of 0.22 cm^2.

TABLE 1. Dye-Sensitized Solar Cell Performance[a]

support/dye	J_{sc} (mA cm^{-2})	V_{oc} (V)	ff	η (%)
TiO_2/N719	18.28	0.729	0.697	9.29
TiO_2+Au@TiO_2/N719	18.281	0.771	0.694	9.78
TiO_2+Au@SiO_2/N719	20.31	0.727	0.691	10.21

[a] Performances of DSSCs were measured with 0.18 cm^2 working area under AM 1.5 illumination. Electrolyte: 0.6 M DMPImI, 0.05 M I_2, 0.1 M LiI, and 0.5 M *tert*-butylpyridine in acetonitrile. Au@TiO_2 and Au@SiO_2 loadings were kept at 0.7% by weight. ff and η correspond to fill factor and power conversion efficiency, respectively. DMPImI, 0.05 M I_2, 0.1 M LiI, and 0.5 M *tert*-butylpyridine in acetonitrile. Excitation: AM 1.5 white light.

slightly higher IPCE, in agreement with the absorption changes seen in Figure 5B. We have repeated these experiments several times to ensure the validity of the small changes seen in the IPCE spectra. The improved photocurrent response in the visible region, though small, can be attributed to the localized surface plasmon effect. The charging effect if any in these films could not be resolved through these IPCE experiments.

The *J*–*V* characteristics of the DSSC employing three dye-loaded TiO_2 photoanodes are presented in Figure 7A, and the cell parameters are summarized in Table 1. The short-circuit current density (J_{sc}), open-circuit voltage (V_{oc}), fill factor (ff), and overall conversion efficiency (η) of TiO_2+Au@TiO_2/N719 are 18.28 mA cm^{-2}, 771 mV, 0.69, and 9.78%, respectively. For TiO_2+Au@SiO_2/N719, the photovoltaic parameters are 20.31 mA cm^{-2}, 727 mV, 0.69, and 10.21%, respectively. For TiO_2/N719, the photovoltaic parameters are 18.28 mA cm^{-2}, 729 mV, 0.69, and 9.29%, respectively. We also tested all three electrodes without modification with dye (Figure 7B). The small fraction of UV accessible under AM 1.5 irradiation produced relatively small photocurrent and photovoltages. It is interesting to note that except for the magnitude, the trends observed in the photocurrents and photovoltages were similar to those with dye-sensitized films in Figure 7A.

From these results (Figure 7 and Table 1), two distinct features emerge. First, the DSSC employing TiO_2+Au@SiO_2/N719 as photoanode shows an increase in short-circuit current. This increase in photocurrent is consistent with the superior performance seen in the IPCE spectra. On the other hand, the open-circuit voltage of this solar cell (*viz.*, TiO_2+Au@SiO_2 photoanode) is similar to the one employing TiO_2/N719 as photoanode. A distinctively different trend is seen in DSSC that employs TiO_2+Au@TiO_2/N719 as photoanode. The DSSC employing TiO_2+Au@TiO_2/N719 exhibits an increase of 42 mV in open-circuit voltage as compared to the TiO_2/N719 photoanode with no noticeable changes in the photocurrent (Figure 7B). This significant increase in V_{oc} suggests that a mechanism other than plasmon-induced enhancement must be operative in determining the performance of DSSC. As shown in previous sections, the Au@TiO_2 are capable of storing electrons in the metal core, which contributes to the shift in Fermi level of the composite to more negative potential. Indeed, the increase in open-circuit voltage supports such a shift in the Fermi level. The observed shift of 42 mV is in good agreement with the shift (40 mV) in apparent Fermi level observed for 5 nm diameter Au nanoparticles covalently linked to TiO_2 nanoparticles.[34]

Figure 8 shows the dependence of DSSC cell parameters (short-circuit current density (J_{sc}), open-circuit voltage (V_{oc}), fill factor (ff), and overall conversion efficiency (η)) on the loading of Au@SiO_2 and Au@TiO_2 in mesoscopic TiO_2 films. These experiments conducted as a separate set allowed us to optimize the performance as well as distinguish the role of core–shell nanoparticles in DSSC. It is interesting note that increasing the Au@SiO_2 concentration results in increased photocurrent with no significant influence on the open-circuit voltage. At loadings greater than 0.7% we see a decrease in photocurrent, probably caused by the filtering effects caused by the Au core.

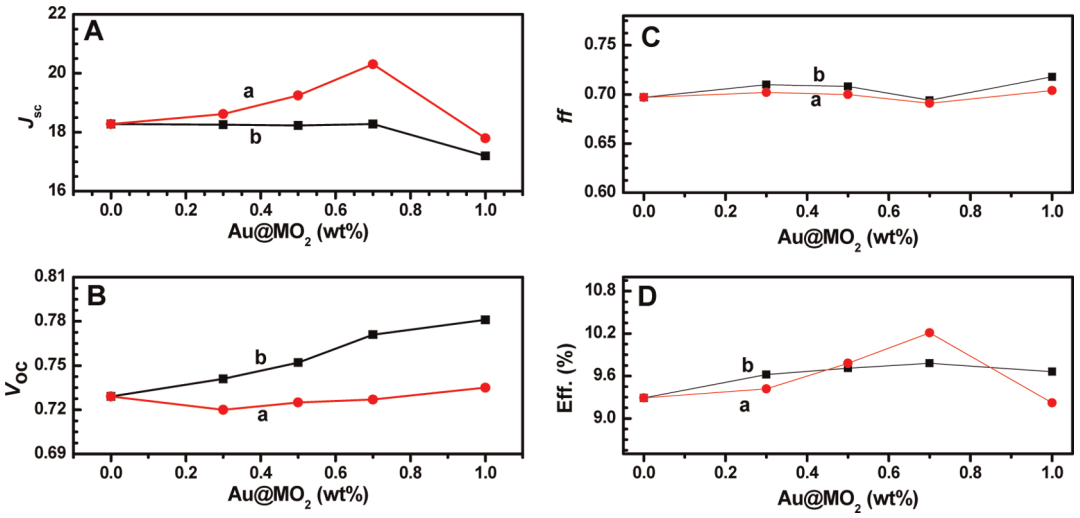

Figure 8. Dependence of DSSC cell parameters on the concentration of core–shell particles: (A) short-circuit current (J_{sc}), (B) open-circuit voltage (V_{oc}), (C) fill factor (ff), and (D) overall power conversion efficiency (η) under AM 1.5 illumination. Traces (a) and (b) correspond to the loading of Au@SiO_2 and Au@TiO_2 nanoparticles into the mesoscopic TiO_2 film. All films were sensitized with N719 dye.

The Au@TiO_2, on the other hand, exhibited relatively smaller enhancement in the photocurrent. The increase in photovoltage was responsive to the neighboring Au@TiO_2 and not to Au@SiO_2, confirming the observations in Table 1 and Figure 7. Given the DSSC employed in the present experiment is a high-efficency cell, the fill factor essentially remained unchanged around 0.7.

In the case of Au@SiO_2 the enhancement in photoelectrochemical performance is exclusively attributed to the influence of localized surface plasmon effect. However, in the case of films containing Au@TiO_2, both charging and LSP are in play. In an earlier study, Snaith and co-workers observed an increase in power conversion efficiency of DSSC from 1.2% to 2.2% after incorporating 0.7% Au@SiO_2 nanoparticles in the TiO_2 film.[11] In another study Qi *et al.*[13] observed an increase from 3.1% to 4.4%. for 0.6% loading of Ag@TiO_2 and 7.8% to 9.0% for 0.1% loading of Ag@TiO_2 in DSSC. Since these two studies were carried out under different experimental conditions, it is difficult to make a direct comparison to distinguish the participation of plasmonic metal@oxide nanoparticles. The comparisons of overall efficiency with similar size core but different shell plasmonic Au nanoparticles allowed us to compare their influence on overall efficiency. DSSC employing Au@TiO_2 and Au@SiO_2 exhibit higher efficiency than pristine TiO_2 as support, thus confirming the influence of metal nanoparticles in boosting the efficiency (Table 1).

The increased power conversion efficiency (η) of DSSC with Au@SiO_2, which exclusively provides a plasmon resonance effect, yields nearly 10% higher power conversion efficiency. This increase in efficiency is in line with the increase observed in an earlier study.[11] The higher photocurrent essentially arises from the improved charge separation and increased absorption of the incident light. Despite the higher V_{oc} observed with Au@TiO_2, the overall increase in power conversion efficiency, η, is about 5%, slightly less than that observed with Au@SiO_2. These results suggest that the charging effects seen in Au@TiO_2 seem to minimize the plasmonic influence in DSSC. Although the Au core in both these cases is similar, the surrounding oxide shell results in the difference in its influence. Au@TiO_2 particles undergo charge equilibration with the neighboring TiO_2 nanoparticles, which in turn assist in maintaining a more negative Fermi level.

Obviously, the charge equilibration between metal nanoparticle and semiconductor remains an important contributor, and its influence cannot be ignored. At present limited information is available to explain the counterintuitive effects of plasmonic and charging effects.

Plasmonic *versus* Charging Effect in DSSC. Metal particles have been known to play an important role as cocataylsts in semiconductor-assisted photocatalytic reduction processes. The ability of metal nanoparticles to accept electrons and promote interfacial charge transfer has been well studied.[7,28,29,59–61] Hence, it is important to take into account this property when considering light-harvesting systems composed of metal nanoparticles directly in contact with semiconductor nanostructures. Recent reports have attributed enhancement in the performance of semiconductor–metal composite based photocatalysts or solar cells exclusively to plasmon-induced effects.[13,46,48,50–52] In the majority of these cases the evidence for plasmon-induced enhancement includes the increase in absorption cross section and/or corresponding enhancement in photoconversion efficiency. Can such results alone explain the plasmon-induced effect or should other

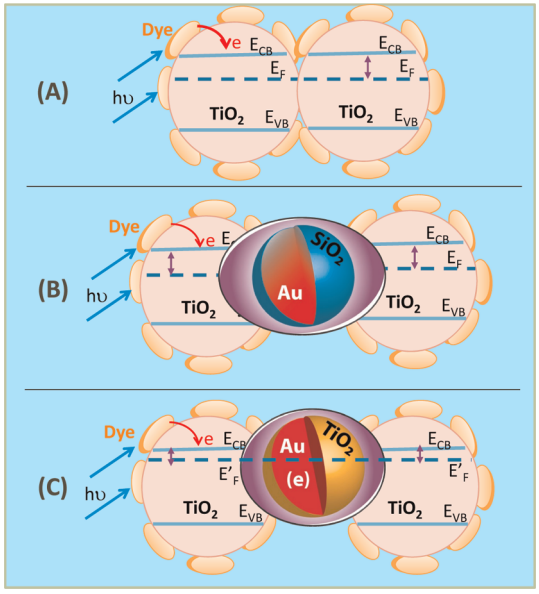

Scheme 3. Electron equilibration and its influence on the apparent Fermi level (E_F): (A) dye−TiO_2 (B) dye−TiO_2/Au@SiO_2, and (C) dye−TiO_2/Au@TiO_2. Note that LSP influence is seen in both (B) and (C), and shift in Fermi level as a result of electron accumulation in the metal core is seen in only (C)

factors associated with semiconductor−metal interactions be taken into account? As shown in the present study, capping with a TiO_2 and a SiO_2 shell provides a convenient way to assess the role of metal nanoparticles in DSSC.

The three scenarios corresponding to the experiments presented in Table 1 are illustrated in Scheme 3. In the case of normal DSSC one observes charge injection from the excited dye into TiO_2 nanoparticles followed by the transport of electrons to the collecting electrode surface. When Au@SiO_2 is present as a neighbor, the influence is mainly limited to localized plasmonic effects, resulting in better charge separation. Note that such LSP does not alter the apparent Fermi level of the composite film. If Au is in contact with a TiO_2 nanoparticle or nanoshell, it is capable of accepting electrons from the neigboring TiO_2/dye particles and undergoing Fermi level equilibration. Such Fermi level equilibration and shift of the apparent Fermi level to more negative potential are reflected as an increase in the open-circuit voltage of the DSSC. Indeed, a closer look at earlier reported plasmonic DSSC papers[13] that employ a Ag -capped TiO_2 system shows a clear increase in open-circuit potential of about 50−100 mV. The results discussed in this work highlight the need to consider charging of the metal core in addition to localized surface plasmon effects.

Concluding Remarks. It is important that the metal nanoparticles introduced as a friendly neighbor in a semiconductor -based assembly can influence the overall photocatalytic or photovoltaic performance in more than one way. Whereas plasmonic effects induced by gold nanoparticles play an important role, other effects such as electron storage could coexist and in fact dominate in many instances. The examples discussed in the present study provide a convenient way to isolate the two effects. The surface plasmon resonance effects increase the photocurrent of DSSC, while the charging effects lead to an increase in photovoltage. These observations open up new opportunities to introduce both these paradigms and synergetically enhance the photocurrent and photovoltage of DSSC. Experiments are under way to optimize these two core@shell structures in DSSC and explore their synergy in further improving the efficiency.

EXPERIMENTAL SECTION

Materials. All reactions were carried out under a nitrogen atmosphere. Solvents were distilled from appropriate reagents.

Synthesis of Oleylamine-Capped Gold Nanoparticles. The Au core nanoparticles were prepared using a two-phase synthesis method with minor modifications.[62] A 50 mL amount of a 10 mM $HAuCl_4$ solution was prepared in H_2O and then mixed with 50 mL of a toluene solution containing 25 mM TOAB. After all Au precursors were transferred into the toluene phase, the water phase was discarded. Then 1.65 mL of oleylamine (capping agent) was added into the Au-TOAB precursor. A 0.283 g portion of $NaBH_4$ dissolved in 15 mL of deionized water was quickly added dropwise with vigorous stirring. The mixture turned deep red, indicating formation of Au nanoparticles. The mixture was used without further purification.

Synthesis of Au@TiO_2 Core/Shell Nanoparticles. For further growth of TiO_2 shells, 10 mM mercaptoacetic acid (MAA) was added into a 1 mM gold nanoparticle suspension and stirred for 15 min to replace the amine functional group with thiol. After that, 80 μL of titanium tetra-isopropoxide as the TiO_2 precursor was added, and the reaction solution was kept near the boiling temperature with a reflux attachment for 3 h. The Au@TiO_2 nanoparticles were collected by adding toluene/ethanol, then centrifuged three times. Finally, the Au@TiO_2 nanoparticles were dried under vacuum at 60 °C.

Synthesis of Au@SiO_2 Core/Shell Nanoparticles. A procedure similar to that for Au@TiO_2 was repeated for SiO_2 shell growth. Instead of MAA, 1 mM (3-mercaptopropyl)trimethoxysilane was added into the Au nanoparticles solution and stirred for 15 min to modify silane molecules for further SiO_2 shell growth. Then, 10 μL of sodium silicate as the SiO_2 precursor was added and reacted at boiling temperature with a reflux system for 3 h. The nanoparticles were collected by adding toluene/ethanol, then centrifuged three times. Finally, the Au@SiO_2 nanoparticles were dried under vacuum at 60 °C.

Optical and Electrochemical Measurements. All experiments were carried out at room temperature. All solutions were deaerated by purging nitrogen or argon. Absorption spectra were measured with a Varian Cary 50-Bio UV−vis spectrophotometer. Transmission electron microscopy (TEM) of Au@TiO_2 and Au@SiO_2 core−shell particles was performed on a Titan 80-300 (FEI Company, 300 kV). Energy dispersive X-ray analysis was performed using the EDX detector coupled to the FEI TEM. A Princeton Applied Research model PARSTAT 2263 was used for recording *I*−*V* characteristics. A Newport Oriel QE kit (QE-PV-SI) was used for measuring IPCE values.

Steady-State Photolysis Experiments. The experiments were conducted by photolyzing a N_2-purged solution with UV−visible light (250 W xenon lamp). A $CuSO_4$ filter was introduced in the path of the light beam to cut off light below the wavelength of 300 nm.

Nanocrystalline Photoanode Preparation. FTO glass plates (Pilkington TEC Glass-TEC 8, Solar 2.3 mm thickness) were cleaned in a detergent solution using an ultrasonic bath for 30 min and rinsed with water and ethanol. The FTO glass plates were immersed in 40 mM $TiCl_4$ (aqueous) at 70 °C for 30 min and washed with water and ethanol. The paste incorporating $Au@MO_2$ (M = Ti, Si) was fabricated with a modified procedure. The $Au@MO_2$ in ethanol solution ($Au@MO_2$ to TiO_2 ratio = 0.7 wt %) was mixed with the TiO_2 paste (Solaronix, Ti-Nanoxide T/SP), followed by stirring for 2 days and sonicating. Then ethanol was removed by rotary evaporator. A transparent nanocrystalline layer on the FTO glass plate was prepared by doctor blade printing the TiO_2 paste (Solaronix, Ti-Nanoxide T/SP) and TiO_2 paste incorporating $Au@MO_2$ and then dried at 25 °C for 2 h. The TiO_2 electrodes were gradually heated under an air flow at 325 °C for 5 min, at 375 °C for 5 min, at 450 °C for 15 min, and at 500 °C for 15 min. A paste for the scattering layer containing 400 nm sized anatase TiO_2 particles (CCIC, PST-400C) was deposited by doctor blade printing and then dried for 2 h at 25 °C. The photoanodes were again gradually heated under an air flow at 325 °C for 5 min, at 375 °C for 5 min, at 450 °C for 15 min, and at 500 °C for 15 min. The photoanodes were treated again by $TiCl_4$ at 70 °C for 30 min and sintered at 500 °C for 30 min.

Solar Cell Fabrication. The dye-sensitized TiO_2 film was used as a photoanode in the solar cell. The FTO plate (Pilkington TEC Glass-TEC 8, Solar 2.3 mm thickness) used for the counter electrodes was cleaned with an ultrasonic bath in H_2O, acetone, and 0.1 M HCl (aq), sequentially. Counter electrodes were prepared by coating with a drop of H_2PtCl_6 solution (2 mg of Pt in 1 mL of ethanol) on the cleaned FTO plate and sintered at 400 °C for 15 min. The dye-adsorbed TiO_2 electrode and Pt-counter electrode were assembled into a sealed sandwich-type cell by heating at 80 °C with a hot-melt ionomer film (Surlyn SX 1170-25, Solaronix) as a spacer between the electrodes. A drop of electrolyte solution (electrolyte of 0.6 M 1,2-dimethyl-3-propylimidazolium iodide, 0.05 M I_2, 0.1 M LiI, and 0.5 M *tert*-butylpyridine in acetonitrile) was placed over a hole drilled in the counter electrode of the assembled cell and was driven into the cell *via* vacuum backfilling. Finally, the hole was sealed using additional Surlyn and a cover glass (0.1 mm thickness).

Conflict of Interest: The authors declare no competing financial interest.

Acknowledgment. The research described herein was supported by the Division of Chemical Sciences, Geosciences, and Biosciences, Office of Basic Energy Sciences of the U.S. Department of Energy, through award DE-FC02-04ER15533. This is contribution number NDRL 4919 from the Notre Dame Radiation Laboratory. We acknowledge Ian Lightcap, Sachidananda Krishnamurthy, Dr. Yung-Jung Hsu, and Joseph Manser for fruitful scientific discussions.

Supporting Information Available: Electron titration experiment, the estimation of stored electrons in $Ag@TiO_2$, energy dispersive X-ray analysis of $Au@TiO_2$ and $Au@SiO_2$ and absorption spectra recorded after visible light irradiation of $Au@TiO_2$ suspension are presented. This material is available free of charge *via* the Internet at http://pubs.acs.org.

REFERENCES AND NOTES

1. Kamat, P. V.; Tvrdy, K.; Baker, D. R.; Radich, J. G. Beyond Photovoltaics: Semiconductor Nanoarchitectures for Liquid Junction Solar Cells. *Chem. Rev.* **2010**, *110*, 6664–6688.
2. Mora-Sero, I.; Bisquert, J. Breakthroughs in The Development of Semiconductor Sensitized Solar Cells. *J. Phys. Chem. Lett.* **2010**, *1*, 3046–3052.
3. Buhbut, S.; Itzhakov, S.; Oron, D.; Zaban, A. Quantum Dot Antennas for Photoelectrochemical Solar Cells. *J. Phys. Chem. Lett.* **2011**, *2*, 1917–1924.
4. Walter, M. G.; Warren, E. L.; McKone, J. R.; Boettcher, S. W.; Mi, Q.; Santori, E. A.; Lewis, N. S. Solar Water Splitting Cells. *Chem. Rev.* **2010**, *110*, 6446–6473.
5. Maeda, K.; Domen, K. Photocatalytic Water Splitting: Recent Progress and Future Challenges. *J. Phys. Chem. Lett.* **2010**, *1*, 2655–2661.
6. Joshi, U. A.; Palasyuk, A.; Arney, D.; Maggard, P. A. Semiconducting Oxides to Facilitate the Conversion of Solar Energy to Chemical Fuels. *J. Phys. Chem. Lett.* **2010**, *1*, 2719–2726.
7. Kamat, P. V. Manipulation of Charge Transfer across Semiconductor Interface. A Criterion That Cannot be Ignored in Photocatalyst Design. *J. Phys. Chem. Lett.* **2012**, *3*, 663–672.
8. Teoh, W. Y.; Scott, J. A.; Amal, R. Progress in Heterogeneous Photocatalysis: From Classical Radical Chemistry to Engineering Nanomaterials and Solar Reactors. *J. Phys. Chem. Lett.* **2012**, 629–639.
9. Standridge, S. D.; Schatz, G. C.; Hupp, J. T. Toward Plasmonic Solar Cells: Protection of Silver Nanoparticles *via* Atomic Layer Deposition of TiO_2. *Langmuir* **2009**, *25*, 2596–2600.
10. Nishijima, Y.; Ueno, K.; Yokota, Y.; Murakoshi, K.; Misawa, H. Plasmon-Assisted Photocurrent Generation from Visible to Near-Infrared Wavelength Using a Au-Nanorods/TiO_2 Electrode. *J. Phys. Chem. Lett.* **2010**, *1*, 2031–2036.
11. Brown, M. D.; Suteewong, T.; Kumar, R. S. S.; D'Innocenzo, V.; Petrozza, A.; Lee, M. M.; Wiesner, U.; Snaith, H. J. Plasmonic Dye-Sensitized Solar Cells Using Core@Shell Metal@Insulator Nanoparticles. *Nano Lett.* **2011**, *11*, 438–445.
12. Li, M.; Cushing, S. K.; Wang, Q.; Shi, X.; Hornak, L. A.; Hong, Z.; Wu, N. Size-Dependent Energy Transfer between CdSe/ZnS Quantum Dots and Gold Nanoparticles. *J. Phys. Chem. Lett.* **2011**, *2*, 2125–2129.
13. Qi, J.; Dang, X.; Hammond, P. T.; Belcher, A. M. Highly Efficient Plasmon-Enhanced Dye-Sensitized Solar Cells through Metal@Oxide Core@Shell Nanostructure. *ACS Nano* **2011**, *5*, 7108–7116.
14. Thomann, I.; Pinaud, B. A.; Chen, Z.; Clemens, B. M.; Jaramillo, T. F.; Brongersma, M. L. Plasmon Enhanced Solar-to-Fuel Energy Conversion. *Nano Lett.* **2011**, *11*, 3440–3446.
15. Kraeutler, B.; Bard, A. J. Heterogeneous Photocatalytic Preparation of Supported Catalysts. Photodeposition of Platinum on TiO_2 Powder and Other Substrates. *J. Am. Chem. Soc.* **1978**, *100*, 4317–8.
16. Meisel, D. Catalysis of Hydrogen Production in Irradiated Aqueous Solutions by Gold Sols. *J. Am. Chem. Soc.* **1979**, *101*, 6133–6135.
17. Matsumura, M.; Saho, Y.; Tsubomura, H. Photocatalytic Hydrogen Production from Solutions of Sulfite Using Platinized Cadmium Sulfide Powder. *J. Phys. Chem.* **1983**, *87*, 3807–3808.
18. Matheson, M. S.; Lee, P. C.; Meisel, D.; Pelizzetti, E. Kinetics of Hydrogen Production from Methyl Viologen Radicals on Colloidal Platinum. *J. Phys. Chem.* **1983**, *87*, 394–399.
19. Aspnes, D. E.; Heller, A. Photoelectrochemical Hydrogen Evolution and Water-Photolyzing Semiconductor Suspensions: Properties of Platinum Group Metal Catalyst-Semiconductor Contacts in Air and in Hydrogen. *J. Phys. Chem.* **1983**, *87*, 4919–4929.
20. Henglein, A. Small-Particle Research: Physicochemical Properties of Extremely Small Colloidal Metal and Semiconductor Particles. *Chem. Rev.* **1989**, *89*, 1861–1873.
21. Henglein, A. Physicochemical Properties of Small Metal Particles in Solution: "Microelectrode" Reactions, Chemisorption, Composite Metal Particles, and the Atom-to-Metal Transition. *J. Phys. Chem.* **1993**, *97*, 5457–5471.
22. Nosaka, Y.; Yamaguchi, K.; Kuwabara, A.; Miyama, H.; Baba, R.; Fujishima, A. Colloidal CdS-Pt Photocatalyst Stabilized by Pendant Viologen Polymer for Photoinduced Electron Transfer and Hydrogen Evolution. *J. Photochem. Photobiol., A* **1992**, *64*, 375–382.
23. Jin, Z.; Li, Q.; Zheng, X.; Xi, C.; Wang, C.; Zhang, H.; Feng, L.; Wang, H.; Chen, Z.; Jiang, Z. Surface Properties of Pt-CdS

and Mechanism of Photocatalytic Dehydrogenation of Aqueous Alcohol. *J. Photochem. Photobiol., A* **1993**, *71*, 85–96.
24. Kamat, P. V. Photophysical, Photochemical and Photocatalytic Aspects of Metal Nanoparticles. *J. Phys. Chem. B* **2002**, *106*, 7729–7744.
25. Kudo, A.; Miseki, Y. Heterogeneous Photocatalyst Materials for Water Splitting. *Chem. Soc. Rev.* **2009**, *38*, 253–278.
26. Shankar, K.; Basham, J. I.; Allam, N. K.; Varghese, O. K.; Mor, G. K.; Feng, X.; Paulose, M.; Seabold, J. A.; Choi, K.-S.; Grimes, C. A. Recent Advances in the Use of TiO_2 Nanotube and Nanowire Arrays for Oxidative Photoelectrochemistry. *J. Phys. Chem. C* **2009**, *113*, 6327–6359.
27. Ng, Y. H.; Iwase, A.; Kudo, A.; Amal, R. Reducing Graphene Oxide on a Visible-Light $BiVO_4$ Photocatalyst for an Enhanced Photoelectrochemical Water Splitting. *J. Phys. Chem. Lett.* **2010**, *1*, 2607–2612.
28. Harris, C.; Kamat, P. V. Photocatalytic Events of CdSe Quantum Dots in Confined Media. Electrodic Behavior of Coupled Platinum Nanoparticles. *ACS Nano* **2010**, *4*, 7321–7330.
29. Takai, A.; Kamat, P. V. Capture, Store and Discharge. Shuttling Photogenerated Electrons Across TiO_2-Silver Interface. *ACS Nano* **2011**, *4*, 7369–7376.
30. Oldfield, G.; Ung, T.; Mulvaney, P. Au@SnO_2 Core-Shell Nanocapacitors. *Adv. Mater.* **2000**, *12*, 1519–1522.
31. Chapman, R.; Mulvaney, P. Electro-Optical Shifts in Silver Nanoparticle Films. *Chem. Phys. Lett.* **2001**, *349*, 358–362.
32. Wood, A.; Giersig, M.; Mulvaney, P. Fermi Level Equilibration in Quantum Dot-Metal Nanojunctions. *J. Phys. Chem. B* **2001**, *105*, 8810–8815.
33. Subramanian, V.; Wolf, E. E.; Kamat, P. V. Green Emission to Probe Photoinduced Charging Events in ZnO-Au Nanoparticles. Charge Distribution and Fermi-Level Equilibration. *J. Phys. Chem. B* **2003**, *107*, 7479–7485.
34. Subramanian, V.; Wolf, E. E.; Kamat, P. V. Catalysis with TiO_2/Au Nanocomposites. Effect of Metal Particle Size on the Fermi Level Equilibration. *J. Am. Chem. Soc.* **2004**, *126*, 4943–4950.
35. Chen, S.; Ingram, R. S.; Hostetler, M. J.; Pietron, J. J.; Murray, R. W.; Schaaff, T. G.; Khoury, J. T.; Alvarez, M. M.; Whetten, R. L. Gold Nanoelectrodes of Varied Size: Transition to Molecule-Like Charging. *Science* **1998**, *280*, 2098–2101.
36. Pietron, J. J.; Hicks, J. F.; Murray, R. W. Using Electrons Stored on Quantized Capacitors in Electron Transfer Reactions. *J. Am. Chem. Soc.* **1999**, *121*, 5565–5570.
37. Templeton, A. C.; Wuelfing, W. P.; Murray, R. W. Monolayer Protected Cluster Molecules. *Acc. Chem. Res.* **2000**, *33*, 27–36.
38. Sudeep, P. K.; Takechi, K.; Kamat, P. V. Harvesting Photons in the Infrared. Electron Injection from Excited Tricarbocyanine dye (IR 125) into TiO_2 and Ag@TiO_2 Core-Shell Nanoparticles. *J. Phys. Chem. C* **2007**, *111*, 488–494.
39. Novo, C.; Mulvaney, P. Charge-Induced Rayleigh Instabilities in Small Gold Rods. *Nano Lett.* **2007**, *7*, 520–524.
40. Hirakawa, T.; Kamat, P. V. Charge Separation and Catalytic Activity of Ag@TiO_2 Core-Shell Composite Clusters under UV-Irradiation. *J. Am. Chem. Soc.* **2005**, *127*, 3928–3934.
41. Alvarez-Puebla, R.; Liz-Marzan, L. M.; Garcia de Abajo, F. J. Light Concentration at the Nanometer Scale. *J. Phys. Chem. Lett.* **2010**, *1*, 2428–2434.
42. Nabika, H.; Takase, M.; Nagasawa, F.; Murakoshi, K. Toward Plasmon-Induced Photoexcitation of Molecules. *J. Phys. Chem. Lett.* **2010**, *1*, 2470–2487.
43. Koh, A. L.; Fernaíndez-Domiínguez, A. I.; McComb, D. W.; Maier, S. A.; Yang, J. K. W. High-Resolution Mapping of Electron-Beam-Excited Plasmon Modes in Lithographically Defined Gold Nanostructures. *Nano Lett.* **2011**, *11*, 1323–1330.
44. Slaughter, L.; Chang, W.-S.; Link, S. Characterizing Plasmons in Nanoparticles and Their Assemblies with Single Particle Spectroscopy. *J. Phys. Chem. Lett.* **2011**, *2*, 2015–2023.
45. Blaber, M. G.; Henry, A.-I.; Bingham, J. M.; Schatz, G. C.; Van Duyne, R. P. LSPR Imaging of Silver Triangular Nanoprisms: Correlating Scattering with Structure Using Electrodynamics for Plasmon Lifetime Analysis. *J. Phys. Chem. C* **2012**, *116*, 393–403.
46. Thimsen, E.; Le Formal, F.; Gratzel, M.; Warren, S. C. Influence of Plasmonic Au Nanoparticles on the Photoactivity of Fe_2O_3 Electrodes for Water Splitting. *Nano Lett.* **2011**, *11*, 35–43.
47. Noguez, C. Surface Plasmons on Metal Nanoparticles:The Influence of Shape and Physical Environment. *J. Phys. Chem. C* **2007**, *111*, 3806–3819.
48. Standridge, S. D.; Schatz, G. C.; Hupp, J. T. Distance Dependence of Plasmon-Enhanced Photocurrent in Dye-Sensitized Solar Cells. *J. Am. Chem. Soc.* **2009**, *131*, 8407–8408.
49. Kulkarni, A. P.; Noone, K. M.; Munechika, K.; Guyer, S. R.; Ginger, D. S. Plasmon-Enhanced Charge Carrier Generation in Organic Photovoltaic Films Using Silver Nanoprisms. *Nano Lett.* **2010**, *10*, 1501–1505.
50. Gao, H.; Liu, C.; Jeong, H. E.; Yang, P. Plasmon-Enhanced Photocatalytic Activity of Iron Oxide on Gold Nanopillars. *ACS Nano* **2012**
51. Awazu, K.; Fujimaki, M.; Rockstuhl, C.; Tominaga, J.; Murakami, H.; Ohki, Y.; Yoshida, N.; Watanabe, T. A Plasmonic Photocatalyst Consisting of Silver Nanoparticles Embedded in Titanium Dioxide. *J. Am. Chem. Soc.* **2008**, *130*, 1676–1680.
52. Liu, Z.; Hou, W.; Pavaskar, P.; Aykol, M.; Cronin, S. B. Plasmon Resonant Enhancement of Photocatalytic Water Splitting Under Visible Illumination. *Nano Lett.* **2011**, *11*, 1111–1116.
53. Warren, S. C.; Walker, D. A.; Grzybowski, B. A. Plasmoelectronics: Coupling Plasmonic Excitation with Electron Flow. *Langmuir* **2012**, *28*, ASAP doi:10.1041/la300377j.
54. Gomez, D. E.; Vernon, K. C.; Mulvaney, P.; Davis, T. J. Surface Plasmon Mediated Strong Exciton-Photon Coupling in Semiconductor Nanocrystals. *Nano Lett.* **2009**, *10*, 274–278.
55. Achermann, M. Exciton-Plasmon Interactions in Metal-Semiconductor Nanostructures. *J. Phys. Chem. Lett.* **2010**, *1*, 2837–2843.
56. Kelly, K. L.; Coronado, E.; Zhao, L. L.; Schatz, G. C. The Optical Properties of Metal Nanoparticles: The Influence of Size, Shape, and Dielectric Environment. *J. Phys. Chem. B* **2003**, *107*, 668–677.
57. Sun, Y.; Gray, S. K.; Peng, S. Surface Chemistry: a Non-Negligible Parameter in Determining Optical Properties of Small Colloidal Metal Nanoparticles. *Phys. Chem. Chem. Phys.* **2011**, *13*, 11814–11826.
58. Henglein, A.; Lilie, J. Storage of Electrons in Aqueous Solution: The Rates of Chemical Charging and Discharging The Colloidal Silver Microelectrode. *J. Am. Chem. Soc.* **1981**, *103*, 1059–66.
59. Ohtani, B.; Kakimoto, M.; Nishimoto, S.; Kagiya, T. Photocatalytic Reaction of Neat Alcohols by Metal-Loaded Titanium(IV) Oxide Particles. *J. Photochem. Photobiol. A: Chem.* **1993**, *70*, 265–272.
60. Bamwenda, G. R.; Tsubota, S.; Nakamura, T.; Haruta, M. Photoassisted Hydrogen-Production from a Water-Ethanol Solution−A Comparison of Activities of Au-TiO_2 and Pt-TiO_2. *J. Photochem. Photobiol. A: Chem.* **1995**, *89*, 177–189.
61. Amirav, L.; Alivisatos, A. P. Photocatalytic Hydrogen Production with Tunable Nanorod Heterostructures. *J. Phys. Chem. Lett.* **2010**, *1*, 1051–1054.
62. Brust, M.; Walker, M.; Bethell, D.; Schffrin, D. J.; Whyman, R. Synthesis of Thiol-Derivatized Gold Nanoparticles in a Two-Phase Liquid-Liquid System. *J. Chem. Soc., Chem. Commun.* **1994**, 801–802.